Double-degenerate Fermi mixtures of ^{6}Li and ^{53}Cr atoms

A. Ciamei,[1,2,*] S. Finelli [1,2,3] A. Cosco,[3] M. Inguscio,[1,2,4] A. Trenkwalder,[1,2] and M. Zaccanti [1,2]

[1]*Istituto Nazionale di Ottica, Consiglio Nazionale delle Ricerche, 50019 Sesto Fiorentino, Italy*
[2]*European Laboratory for Non-Linear Spectroscopy, Università di Firenze, 50019 Sesto Fiorentino, Italy*
[3]*Dipartimento di Fisica e Astronomia, Università di Firenze, 50019 Sesto Fiorentino, Italy*
[4]*Department of Engineering, Campus Bio-Medico University of Rome, 00128 Rome, Italy*

We report on the realization of a degenerate mixture of ultracold fermionic lithium and chromium atoms. Based on an all-optical approach, with an overall duty cycle of about 13 s, we produce large and degenerate samples of more than 2×10^5 ^{6}Li atoms and 10^5 ^{53}Cr atoms, with both species exhibiting normalized temperatures of about $T/T_F = 0.25$. Additionally, through the exploitation of a crossed bichromatic optical dipole trap, we can controllably vary the density and degree of degeneracy of the two components almost independently and widely tune the lithium-to-chromium density ratio. Our ^{6}Li - ^{53}Cr Fermi mixture opens the way to the investigation of a variety of exotic few- and many-body regimes of quantum matter and it appears as an optimally suited system to realize ultracold paramagnetic polar molecules, characterized by both electric and magnetic dipole moments. Ultimately, our strategy also provides an efficient pathway to produce dipolar Fermi gases, or spin mixtures, of ultracold ^{53}Cr atoms.

I. INTRODUCTION

Quantum matter composed of unequal kinds of fermionic particles, such as quarks of different colors or electrons belonging to different lattice bands, is known to promote a plethora of exotic phenomena [1–6], qualitatively distinct from those characterizing single-component systems. The combination of quantum statistics with a mass asymmetry and a distinct response to external fields of two different fermionic species indeed provides an increased level of complexity, with a strong impact at both the few- and many-body levels. In this context, heteronuclear Fermi mixtures of ultracold atoms, resonantly interacting close to a Feshbach resonance [7], are regarded as clean and versatile frameworks optimally suited for the disclosure of exotic few-particle states [8–20] and the exploration of novel quantum phases, primarily in the context of unconventional superfluid pairing [21–31] and quantum magnetism [32–36].

In particular, Fermi mixtures with mass ratios $8.17 \lesssim M/m \lesssim 13.6$ are especially appealing from a few-particle physics perspective, as they are predicted to support, already in three dimensions, non-Efimovian few-body cluster states, completely unexplored thus far, which exhibit universal character and a peculiar p-wave orbital symmetry [9,13,15,18,37]. These elusive states are extremely relevant also from a many-body viewpoint, in light of their collisional stability. In fact, owing to the *halo* nature of such non-Efimovian clusters, largely exceeding in size the van der Waals range of the interatomic interaction potential, their existence does not trigger an increase of inelastic decay processes [38], in stark contrast to the widely explored Efimovian case [39]. Therefore, the presence of fermionic trimers [9,13,15] and bosonic tetramers

[18,37], expected to exist for $8.17 \lesssim M/m \lesssim 13.6$ [9] and $8.86 \lesssim M/m \lesssim 13.6$ [18], respectively, may uniquely allow one to experimentally attain qualitatively new many-body regimes, within which strong few-body correlations add to, or may even overcome, the standard two-body ones. However, none of the Fermi-Fermi mixtures nowadays available, i.e., ^{6}Li - ^{40}K [40–42], ^{40}K - ^{161}Dy [43,44], and ^{6}Li - ^{173}Yb [45,46], exhibits a mass ratio that allows one to probe such an appealing scenario, although related few-body effects have been disclosed in Li-K [47].

Here we report on the realization of a degenerate Fermi mixture made of ^{6}Li alkali-metal and ^{53}Cr transition-metal ultracold atoms. Our interest for this new system is three-fold. First, the peculiar chromium-lithium mass ratio, of about 8.8, is extremely close to the critical values above which both three- and four-body non-Efimovian states are predicted to emerge [9,13,15,18,37]. This feature, combined with the recent discovery of various magnetic Feshbach resonances well suited to control Li-Cr interactions [48], makes such a biatomic combination an unparalleled framework with which to explore a different class of *elastic* few-body effects and their impact at the many-body level [15,18]. Second, in the regime of strong repulsive interactions, three-body recombination processes are predicted to be drastically suppressed for the specific Li-Cr mass ratio [49], lithium-chromium Fermi mixtures thus representing a pristine platform to explore Stoner's ferromagnetism [50] and related phenomena [51–55], immune to the pairing instability. Finally, recent *ab initio* calculations [56] foresee, for the ground state of the LiCr dimer, a sizable electric dipole moment of about 3.3 D, combined with an $S = 5/2$ electronic spin, thereby making Li-Cr mixtures also extremely appealing candidates to realize ultracold paramagnetic polar molecules.

Our strategy to produce degenerate lithium-chromium Fermi mixtures is formally similar to the all-optical one
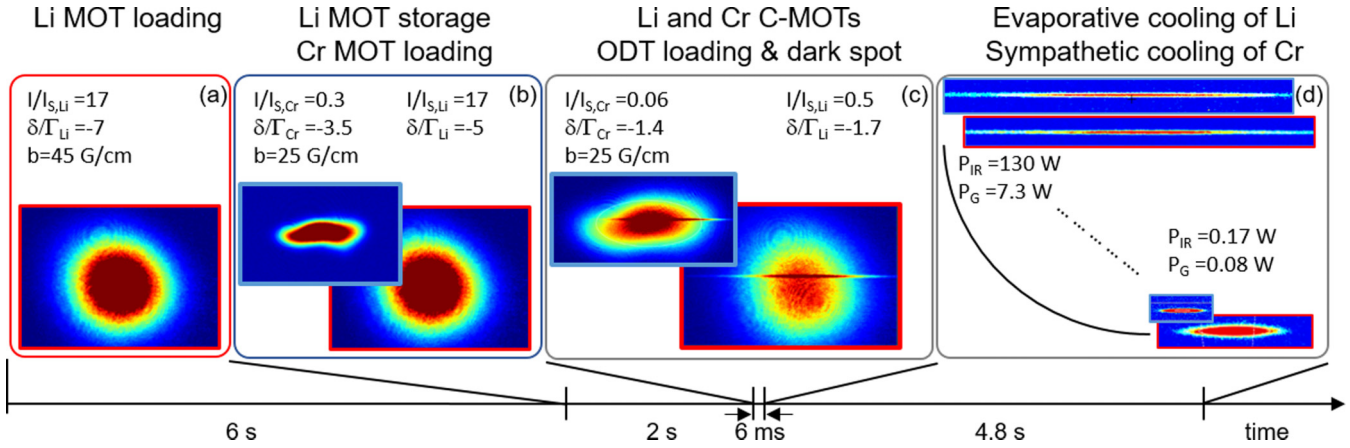
*ciamei@lens.unifi.it

FIG. 1. Schematic overview of the experimental routine discussed in the text. Our protocol consists of the following main steps: (a) and (b) sequential loading of a cold Li-Cr mixture in a dual-species magneto-optical trap, (c) efficient collection of the two components into a bichromatic optical dipole trap through the implementation of a dark spot for the chromium MOT, and (d) evaporative cooling of a two-state lithium mixture and simultaneous sympathetic cooling of chromium. Optimized values of the most relevant experimental parameters are specified for each stage. Typical absorption images, acquired at the end of each step of the routine, are shown for the two mixture components, with Li (Cr) images being framed in red (blue). The timeline of the experimental cycle, overall lasting 12.8 s, is shown below the panels.

developed for the lithium-potassium system in the experiment of Spiegelhalder *et al.* [57] and it consists of the following main steps, summarized in Fig. 1: (i) realization of a cold mixture in a dual-species magneto-optical trap (MOT) [58], (ii) direct loading of the two components into an optical dipole trap, and (iii) evaporative cooling of a two-state lithium mixture and simultaneous sympathetic cooling of chromium. In spite of its conceptual simplicity, successful application of this approach to Li-Cr mixtures requires tackling various challenges, mostly connected with fermionic chromium and its rather limited experimental investigation [58–60]. Specifically, a few major issues make the production of ultracold ^{53}Cr gases nontrivial. First, chromium suffers from rather strong light-assisted inelastic collisions [59], which has so far limited the ^{53}Cr number collected in the MOT to roughly 10^6 [58]. Second, direct loading of chromium atoms from the MOT into an infrared optical dipole trap has proved challenging, owing to detrimental light shifts [61,62]. Finally, efficient sympathetic cooling of chromium with lithium should not be taken for granted. Although the Li-Cr background scattering length, of about $42a_0$ [48], is close to the Li-K one [40,63] and thus sufficient to guarantee a good thermalization rate, efficient Li-Cr sympathetic cooling in a standard 1070-nm optical trap is hard to achieve, given that the chromium polarizability is about 1/3 of the lithium one, in contrast with a potassium-to-lithium polarizability ratio of about 2 at such a wavelength [57].

In the following, we describe how we could overcome these challenges in the experiment, obtaining degenerate samples comprising more than 2×10^5 Li and 10^5 Cr atoms, polarized in their lowest Zeeman states, at temperatures of about 200 nK, corresponding to $T/T_{F,\text{Li}} \sim T/T_{F,\text{Cr}} \sim 0.25$.[1]

The paper is organized as follows. In Sec. II we describe our new protocol to produce a dual-species Li-Cr MOT. In particular, we discuss how the ^{53}Cr MOT atom number can be substantially increased with respect to previous studies [58,59], reaching up to 8×10^7 within a 2-s loading time and in the presence of a MOT of 10^9 ^{6}Li atoms. In Sec. III we present an efficient scheme to load simultaneously Li and Cr atoms in a bichromatic optical dipole trap (BODT) directly from the MOT, based on the implementation of a dark spot, obtained through a weak green beam at 532 nm superimposed onto the main trapping beam at 1073 nm [64]. In Sec. IV we show the evaporation trajectories followed by the two components and in particular how the sympathetic cooling efficiency at ultralow temperatures can be substantially increased by exploiting a narrow interspecies Feshbach resonance. In Sec. V we describe how a crossed bichromatic beam, added to our main BODT, allows us to greatly improve the chromium degree of degeneracy and to simultaneously reach deeply degenerate conditions for both atomic components.

II. DUAL SPECIES ^{6}Li - ^{53}Cr MOT

The experimental apparatus employed for the present studies, apart from targeted changes in the optical setup summarized below, has been described in depth in our previous work [58], to which we refer the reader for more details. To produce the lithium MOT, we essentially follow the scheme developed in Ref. [65]. Laser cooling and trapping of such an element is well established and it requires only two laser lights addressing the D_2 ($^2S_{1/2} \to ^2P_{3/2}$) atomic line at 671 nm: the cooling light, addressing the $F = 3/2 \to F' = 5/2$ transition, and the repumper light, detuned by 228 MHz from the cooling one, nearly resonant with the $F = 1/2 \to F' = 3/2$ transition. With respect to the Li MOT performance we previously reported [58], a further optimized shaping of both MOT and Zeeman slower (ZS) beams allows us to increase the lithium
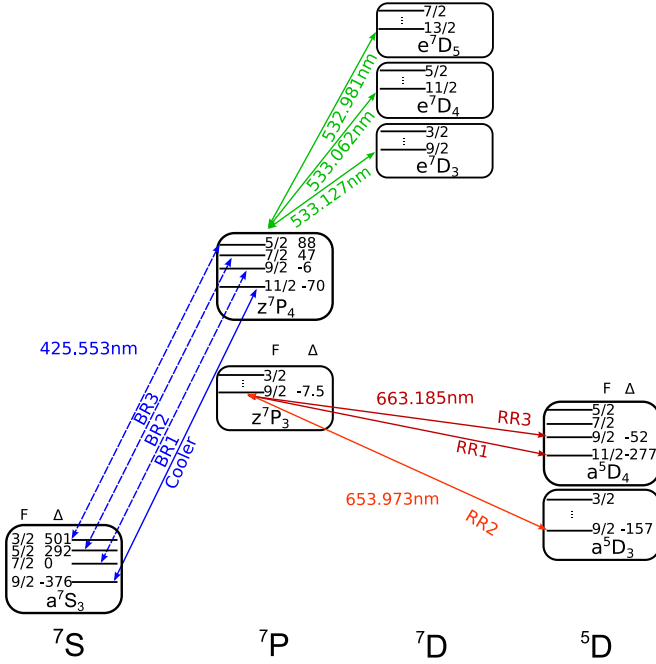
---

[1]Here $T_{F,i} = \hbar\bar{\omega}_i(6N_i)^{1/3}/k_B$ defines the Fermi temperature of a gas of N_i atoms (with $i = \text{Li, Cr}$), trapped in a harmonic potential with average angular frequency $\bar{\omega}_i$.

FIG. 2. Sketch of energy levels and optical transitions addressed for the laser cooling of ^{53}Cr atoms (not to scale). For each relevant hyperfine level originating from the nonzero nuclear spin $I = 3/2$, the F quantum number and the detuning Δ in MHz, referenced to an assumed $I = 0$ state, are shown. A single frequency-doubled laser at 425.5 nm delivers the light exciting atoms from $^7S_3$ to $^7P_4$, addressing the main cooling transition labeled "Cooler" (solid blue), and the repumping transitions denoted by BR_1, BR_2, and BR_3 (dashed blue) in order of decreasing gain on the steady-state MOT number. Metastable ^5D states onto which $^7P_4$ atoms decay by spontaneous emission are repumped back into the cooling cycle by three additional red repumper beams labeled as RR_1, RR_2, and RR_3, with the same indexing used for BR. These lights are delivered by two independent master oscillators at 663 and 654 nm (see Ref. [58] for more details). Here RR_1 and RR_3, detuned from each other by only 225 MHz, are obtained by two separate sets of acousto-optic modulators. The three green transitions around 533 nm, coupling the $^7P_4$ to the $^7D_{3,4,5}$ states, are relevant for the operation of the dark spot discussed in Sec. III.

atom number collected in the MOT from 4×10^8 to 10^9, after a typical loading time of 6 s.

For the ^{53}Cr component, a much more substantial increase in the MOT atom number is achieved here, resulting in an improvement by almost two orders of magnitude relative to previous studies [58,59]. We then devote the rest of this section to describe our upgraded chromium optical setup and, after recalling some theoretical results about the MOT loading dynamics, to discuss our experimental findings and procedures to realize large Cr cold samples, also in combination with the Li component.

A. Improved ^{53}Cr MOT optical setup

As described in Refs. [58,59], laser cooling of fermionic chromium is based on the $^7S_3 \rightarrow {}^7P_4$ ($F_S = 9/2 \rightarrow F_P' = 11/2$) atomic line (see Fig. 2 for a sketch of the energy-level diagram and addressed optical transitions). Besides the cool-

ing light, three blue repumpers, denoted by BR_1, BR_2, and BR_3, respectively, are required to operate the MOT. Furthermore, even with all blue repumpers on, the MOT transition remains slightly leaky, since optically excited atoms can decay from the $^7P_4$ state onto underlying $^5D_3$ and $^5D_4$ metastable states. Therefore, three additional red repumpers, denoted by RR_1, RR_2, and RR_3 in order of repumping efficiency, are needed to fully close the cooling cycle. In particular, RR_3, not implemented in our previous work [58], is introduced here and it leads to a further increase of 10% in the steady-state MOT atom number.

We carefully optimize the size of all laser beams shone on the Cr MOT cloud, with the freedom of changing the power repartition between different beams and under the constraint of a maximum available blue power of 500 mW. In particular, we increase the MOT and repumper beam waists by about a factor of 2 relative to our previous setup [58], now featuring $1/e^2$ radii of about 0.65 cm, effectively increasing the capture volume by almost one order of magnitude. Notably, these improvements on the chromium setup enable us to identify a peculiar region in the detuning-intensity plane of the MOT cooling light, within which light-assisted losses are drastically suppressed, as shown in the following.

B. The ^{53}Cr MOT: A few theoretical considerations

In order to understand our strategy and the experimental data presented below, we recall some textbook results about the loading dynamics in a MOT. Quite generally, the atom number in a MOT follows a time evolution defined by the rate equation

$$\frac{dN}{dt} = \Gamma_L - \alpha N(t) - \frac{\beta}{\langle V \rangle} N^2(t), \tag{1}$$

where Γ_L is the loading rate, α is a one-body decay rate, β is the rate coefficient per unit volume for light-assisted collisions, and $\langle V \rangle$ denotes the density-weighted volume of the cloud. Since in our experiment we exploit all (blue and red) repumping lights, we can neglect the one-body loss term and safely set $\alpha = 0$. Equation (1) then yields the asymptotic value for the collected atom number

$$N_\infty = \sqrt{\frac{\Gamma_L \langle V \rangle}{\beta}}. \tag{2}$$

From Eq. (2) one can immediately see that, in order to increase N_∞, one needs to maximize Γ_L (solely dependent on the transverse cooling and Zeeman slowing parameters but not on the MOT ones), enlarge $\langle V \rangle$, and minimize β.

Let us consider how these two quantities depend upon the normalized detuning δ/Γ and saturation parameter $s_0 = I/I_S$ of the MOT (for the $^7S_3 \rightarrow {}^7P_4$ chromium line, the natural linewidth is $\Gamma = 2\pi \times 5.02$ MHz, and $I_S = 8.52$ mW/cm^2 is the associated saturation intensity). In the limit of $s_0 \ll 1$ and $|\delta| \gg \Gamma$, one obtains that the MOT volume scales as [66]

$$\langle V \rangle \sim \left(\frac{\Gamma}{16\mu' k_L} \right)^{3/2} \frac{(2\delta/\Gamma)^6}{(bs_0)^{3/2}}, \tag{3}$$

where k_L denotes the laser wave vector, b the magnetic-field gradient, and μ' the effective differential magnetic moment for the cooling transition.

The dominant light-assisted loss processes that affect a chromium MOT involve pairs of one ground S- and one excited P-state atom [58,59]. Thus, denoting by Π_P the P-state population, on quite general grounds one expects the rate coefficient to scale as $\beta \propto \Pi_P(1 - \Pi_P)$. Considering the standard result for Π_P for a two-level atom [66], in the low-intensity and large-detuning limit one obtains that, up to a constant,

$$\beta \sim \frac{s_0}{(2\delta/\Gamma)^2}. \tag{4}$$

Combining this dependence of β upon the MOT parameters, with the one for $\langle V \rangle$ given by Eq. (3), one then expects the MOT atom number to feature a scaling of the kind

$$N_\infty \propto \frac{\sqrt{\Gamma_L}}{b^{3/4}} \frac{(\delta/\Gamma)^4}{s_0^{5/4}}. \tag{5}$$

From the overall trend of Eq. (5), one can see how, for a given loading rate Γ_L, light-assisted losses can be mitigated (thereby substantially increasing N_∞) by working at low s_0 values, large detunings, and weak field gradients of the MOT, although a compromise must be found in order to guarantee a sufficiently strong force and high capture velocity of the MOT.

A well-known system, where very strong light-assisted losses are successfully circumvented by following these concepts, is metastable $^4\text{He}^*$ [67,68]: In that case, operating the MOT at large detunings on the order of $|\delta| \sim 40\Gamma$ while keeping large $s_0 > 10$ values to maintain a sufficiently high capture velocity, it is possible to collect more than 10^9 atoms within a few-second loading time. For the ^{53}Cr system, this strategy is challenging to follow. On the one hand, the saturation intensity (linewidth) of chromium is more than 50 times (3 times) larger than the one of He* and the limited amount of blue power available does not allow us to reach $s_0 \gg 1$ without diminishing the performance of transverse cooling and hyperfine pumping stages at the chromium oven [58], thus decreasing Γ_L. Moreover, contrary to metastable He, ^{53}Cr features a rich and rather dense hyperfine spectrum which, in combination with large s_0 and $|\delta|/\Gamma$ values, may allow the cooling light to address undesired transitions. Indeed, the small optimum Zeeman slower detuning and low exit velocity shown in our previous work [58] have already been interpreted as highly sensitive to residual Doppler shifts during the MOT capture. Hence, we opt to follow a strategy opposite to the one of $^4\text{He}^*$, based on minimizing s_0 while keeping relatively small light detunings of a few Γ.

C. The ^{53}Cr MOT: Experimental results

Experimentally, to test the feasibility of the strategy discussed above, we measure the atom number collected in the MOT after a 2-s loading time, exploring different (small) values of s_0. For each s_0 value, the light detuning is scanned until the maximum number is observed. The study is performed by intentionally keeping both Γ_L and b constant. Specifically, we work at a field gradient $b = 25$ G/cm along the vertical direction. In order to better count the collected atoms, at the end of the loading stage we perform a compressed MOT (CMOT) stage lasting about 6 ms, which greatly reduces the cloud size while not affecting the atom number. Then both MOT gradient
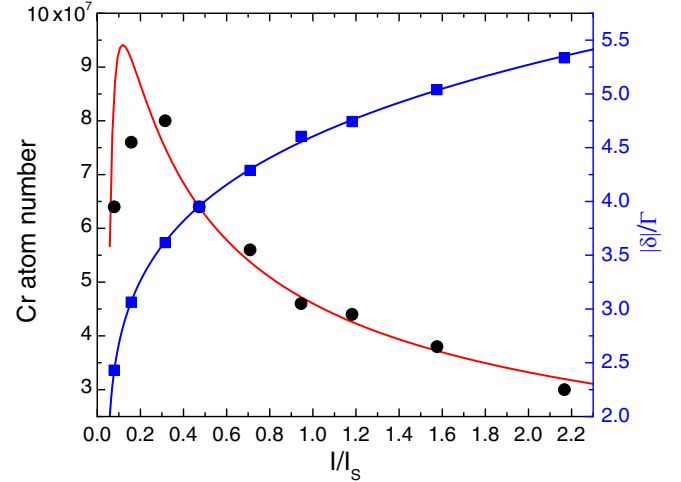

FIG. 3. Characterization of the maximum chromium atom number collected in the MOT after 2 s of loading, as a function of I/I_S (black circles, left axis). Here $I = 2 \times 2P/w^2$ is the peak intensity of one single (retroreflected) MOT beam, characterized by a $1/e^2$ radius $w = 6.5$ mm. Each data point is the average of at least five independent measurements. For each I/I_S, the experimental data exhibit a constant 10% uncertainty. For each value of I/I_S, the corresponding optimum detuning $|\delta|/\Gamma$, experimentally determined, is shown as blue squares, right axis. The blue line shows the best fit to a power law $|\delta|/\Gamma = (I/I_S)^\alpha$ (discussed in text). The red solid line corresponds, up to a multiplicative factor, to N_∞ given by Eq. (5), assuming the best-fitted power-law dependence of $|\delta|/\Gamma$ on I/I_S.

and lights are turned off and an absorption image is acquired after a 2-ms time of flight, from which the atom number is obtained through a two-dimensional Gaussian fit.

Our results are summarized in Fig. 3. The atom number (black circles, left axis) is plotted as a function of the normalized single-beam peak intensity I/I_S, together with the corresponding optimum detuning experimentally identified (blue squares, right axis). One can notice how, throughout the scanned parameter space, a substantial increase in the collected Cr atoms is observed, relative to our previous study [58], and samples ranging from 3×10^7 to 8×10^7 particles can be obtained. The behavior of $|\delta|/\Gamma$ versus s_0 is well fitted to a power law, with exponent $\alpha = 0.22(1)$ (see the blue line). Such a value is relatively close to, but smaller than, the one that would maintain a constant $\beta/\langle V \rangle$ rate for light-assisted collisions in Eq. (5), i.e., $\alpha = 5/16 \sim 0.31$. On the other hand, a nonconstant loss rate is signaled by the observed variation of the MOT atom number (see black circles in Fig. 3). Remarkably, the observed behavior is nicely reproduced by the textbook model expectation (5), shown as a red solid line in Fig. 3, up to a multiplicative constant. The small mismatch between experiment and theory, visible at very low s_0 values, can be ascribed to the fact that in this regime the estimated MOT capture velocity becomes very close to, or even slightly smaller than, the exit velocity of our Zeeman slower. Parallel to that, the MOT size rapidly increases approaching the beam radius, thus making finite-size effects more important.

The identification of a region of MOT parameters able to greatly mitigate light-assisted losses allows us to greatly speed up and simplify the experimental routine to produce a

large ^{6}Li - ^{53}Cr mixture in the cold regime. Since a loading time of 2 s suffices to reach N_∞ for chromium and the MOT performances summarized in Fig. 3 are not affected by the presence of an overlapping lithium cloud, there is no longer a need to pursue accumulation of Cr atoms in magnetically trapped D states [59], a procedure that requires significantly longer loading times and whose efficiency is limited by the presence of a large Li MOT [58]. As a final remark, we note that while the optimum loading conditions summarized in Fig. 3 greatly reduce the Cr MOT density, they do not limit the capture efficiency of the CMOT stage, operated at constant cooling light parameters. As a consequence, the large increase in the MOT atom number directly turns into a significant density increase after the CMOT, hence providing a substantial gain for the successive step of optical trap loading within our experimental routine.

D. Optimized loading of a dual species ^{6}Li - ^{53}Cr MOT

The ability to rapidly collect a large number of ^{53}Cr atoms directly in the MOT allows for an optimized sequential loading of the Li-Cr mixture in our dual-species magneto-optical trap. The most convenient strategy we experimentally identified is summarized as follows. (i) We first load lithium atoms for about 6 s, at an optimum gradient of about $b = 45$ G/cm along the vertical direction. During this time, the chromium lights and ZS field are already on, although a little Cr atom number is collected at this stage. (ii) We switch off the Li Zeeman slower and decrease the MOT gradient down to $b = 25$ G/cm, which is the optimum value found for chromium. The light detuning for lithium is correspondingly slightly diminished to ensure a good storage of this species during the chromium MOT loading. (iii) We operate the Cr MOT for about 2 s with the optimum light parameters reported in Fig. 3. (iv) We then turn off the Cr Zeeman slower (light and field) and adiabatically transfer the cold Li-Cr mixture from the quadrupole field of the MOT coils into that of a smaller set of Feshbach coils [58], yielding the same gradient but allowing for a faster switch off. (v) Finally, a 6-ms-long CMOT phase is applied on both species simultaneously, in order to compress and cool the mixture. This is done, without changing the field gradient, by diminishing the intensity of the MOT lights and moving the cooling frequency closer to resonance. Specifically, for chromium the CMOT detuning is set to about -1.4Γ and the beams intensity is reduced to about 20%, relative to that employed during the loading. For lithium, the detuning is moved from about -7 to -1.7 natural linewidths ($\Gamma_{\text{Li}}/2\pi = 5.87$ MHz) and the light intensity is substantially reduced, passing from more than $17I/I_{S,\text{Li}}$ at the loading stage down to about $0.5I/I_{S,\text{Li}}$ ($I_{S,\text{Li}} = 2.54$ mW/cm^2) [58]. At the end of this procedure, lasting 8 s overall, we obtain cold Li-Cr mixtures comprising 10^9 Li and 8×10^7 Cr atoms, at a temperature of about 300 μK.

III. LOADING OF ^{6}Li - ^{53}Cr MIXTURES INTO A BODT

As anticipated in Sec. I, our experimental strategy is based on an all-optical approach conceptually analogous to the one employed for Li-K mixtures [57]. As a crucial step, this requires an efficient loading of the cold Li-Cr mixture,
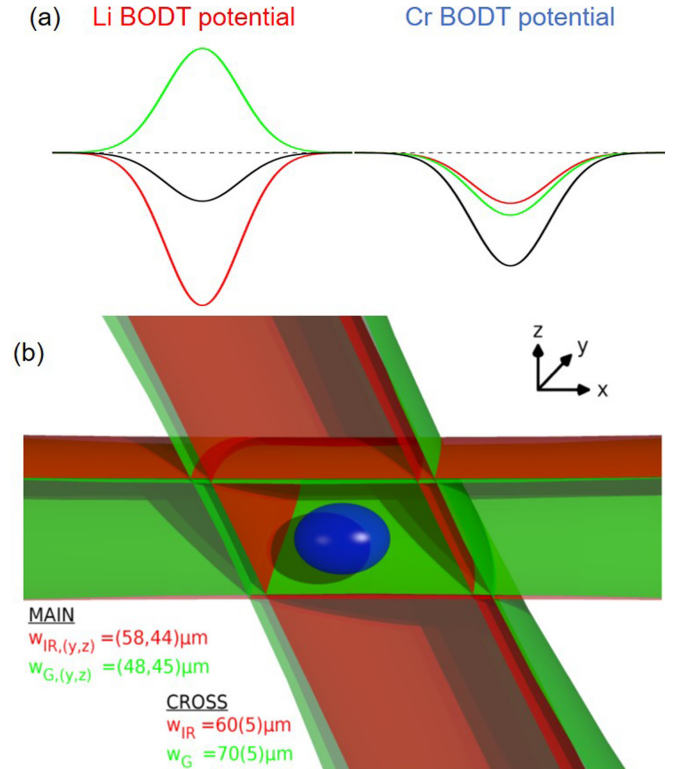

FIG. 4. (a) Sketch of the optical potentials experienced by Li (left) and Cr (right) atoms confined in the BODT. The IR light (red curves) yields a trapping potential about 3.3 times deeper for Li than for Cr atoms, whereas the green beam (green curves) anticonfines lithium and tightly confines chromium (see the text for details). By adjusting the parameters of the two beams, in the figures assumed to feature equal waists and an IR-to-green power ratio of 2, one can obtain an overall BODT potential (black curves) deeper for the Cr than for the Li component. (b) Schematic view of our BODT setup. Two overlapped IR and green beams, propagating in the horizontal plane along the x direction and featuring waists indicated in the figure, provide the primary trapping potential for the atomic mixture, sketched in blue. A secondary bichromatic trap, realized by two additional overlapped IR and green circular beams with waists of about 60 and 70 μm, respectively, crosses the main BODT at an angle of about 15° from the vertical direction. The crossed BODT beam, turned on at the end of the evaporation stage, allows us to tune the densities of the two mixture components independently while not modifying the trap depth (see Sec. V for details).

delivered by our dual-species MOT discussed in Sec. II, into a high-power optical dipole trap. However, also in this case a few factors make the Li-Cr system more challenging than the Li-K one. First, the chromium polarizability for standard infrared (IR) laser trapping lights at 1064 or 1070 nm is only about 30% of the lithium one [see red profiles in Fig. 4(a)], making the resulting IR trap not suited to guarantee an efficient sympathetic cooling of Cr. Indeed, a 1070-nm beam, characterized by power P_{IR} (expressed in watts) and $1/e^2$ waist w_{IR} (in microns), yields a maximum trap depth for lithium and chromium that, expressed in millikelvin, are given by $U_{\text{Li,IR}} \sim -38.3 P_{\text{IR}}/w_{\text{IR}}^2$ and $U_{\text{Cr,IR}} \sim -12.7 P_{\text{IR}}/w_{\text{IR}}^2$, respectively.

We mitigate this issue by superimposing a green beam at 532 nm onto the IR trap. This second light is tightly confining for chromium, whereas it anticonfines lithium [see green profiles in Fig. 4(a)]. Denoting the power and waist of the green beam by P_G and w_G, respectively, one finds in this case $U_{\mathrm{Li},G} \sim +39.2 P_G/w_G^2$ and $U_{\mathrm{Cr},G} \sim -23.5 P_G/w_G^2$. Therefore, by tuning the relative power of the two lights of this bichromatic optical dipole trap, one can control the overall trap depth ratio for the two species [see black profiles in Fig. 4(a)]. Experimentally, the BODT is realized by overlapping our IR trap, already discussed in Ref. [64] and based on a multimode fiber laser module from IPG Photonics (YLR-300) delivering up to 300 W, with a high-power laser at 532 nm. For the latter, we employ a Sprout-G source by Lighthouse Photonics, nominally delivering up to 15 W. The two BODT beams, propagating in the horizontal (x, y) plane, are recombined on a dichroic mirror and then focused onto the center of the Li-Cr MOT clouds, with waists along the vertical (horizontal) directions of $w_{\mathrm{IR},z} = 44$ μm ($w_{\mathrm{IR},y} = 58$ μm) and $w_{G,z} = 45$ μm ($w_{G,y} = 48$ μm) for the IR and green light, respectively.

A second technical problem of Li-Cr is that the direct loading of atoms from the MOT into the optical trap, contrarily to the lithium case (see, e.g., Ref. [65]), has been found to be challenging for chromium [61,62,69]. Besides increasing light-assisted losses owing to an increased density of the trapped cloud, the IR light shifts both $^7S_3$ and $^7P_4$ atomic levels, connected by the main cooling transition, to lower energy, with a shift for the excited state larger than the one of the ground state. Therefore, the detuning $|\delta|$ of the MOT light, experienced by Cr atoms within the IR trap, is effectively reduced (and it may eventually change sign). Light-shift measurements, performed by monitoring the resonance frequency of absorption imaging of a cold Cr cloud in the presence of our IR beam, yields a trap-averaged shift of $-0.021(2)$ MHz/W. This implies that the (C)MOT detuning, experienced by atoms within the IR trap with $P_{\mathrm{IR}} \sim 200$ W, is moved towards resonance by about $+1\Gamma$. It thus becomes almost impossible to simultaneously guarantee a good efficiency of the CMOT stage for Cr atoms both inside and outside the IR trap, especially given the inhomogeneous intensity distribution of the trapping beam. One way to circumvent this problem is to flash the IR trap only once the MOT light is turned off. This, given our large MOT atom number and the high IR power at our disposal, allows us to capture about 10^6 ^{53}Cr atoms within the IR beam at a typical power of 130 W. However, this nonadiabatic loading method considerably heats up the sample and it is far from being optimum also for the lithium component. More involved loading schemes, alternative to the instantaneous flash of the IR trap, have been devised [61,62,69], which rely on the accumulation of metastable D-state atoms in a combined magnetic and optical potential.

In our case, we found a convenient way, offered by our BODT setup, to successfully overcome this major technical issue. The key point is that the 532-nm light dramatically perturbs the cooling transition, owing to the presence of three atomic lines that connect the $^7P_4$ level to the ^7D states (see Fig. 2), all centered around 533 nm and featuring linewidths ranging from 0.9 to about 10 MHz. A relatively weak laser field near 532 nm, blue detuned from these lines by less than 1 nm, thus suffices to greatly shift the $^7S_3 \rightarrow {}^7P_4$ transition
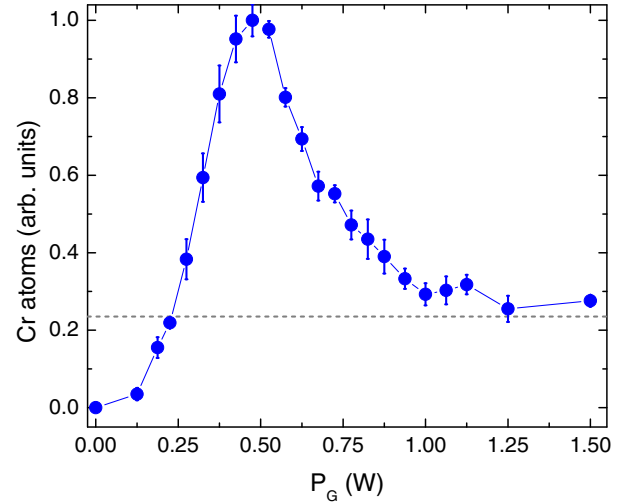

FIG. 5. Characterization of the chromium atom number collected in the BODT directly from the CMOT, as a function of the green beam power acting as a dark spot. The Cr population (blue circles), recorded in the BODT after a hold time of 100 ms through absorption imaging that follows a time-of-flight expansion of 200 μs, is normalized to the maximum value found throughout the scan, centered at 0.47(1) W. Each point corresponds to the average value of at least four independent measurements. Error bars represent the standard deviation of the mean. The horizontal dashed line marks the value obtained by instantaneously flashing the IR trap at the end of the CMOT stage. For this data set, the IR beam has a fixed power of 130 W and the parameters of the CMOT stage are kept constant at their optimum values, obtained in the absence of the BODT. The Sprout-G module used to realize the dark spot has a wavelength of 532.2 nm.

towards higher frequencies. Contrarily to the IR case discussed above, this implies that the effective detuning of the MOT light experienced by atoms within a 532-nm beam is strongly moved out of resonance. The green light of our BODT can thus be efficiently exploited to (over)compensate for the detrimental effect of the IR main beam on the Cr CMOT, realizing an effective dark spot.

We test the feasibility of this loading strategy by increasing the IR beam up to 130 W and simultaneously the green beam to a variable power level, through a 3-ms-long linear ramp that starts 1 ms before the chromium CMOT stage. The laser cooling light parameters are kept fixed to the optimum values experimentally found in the absence of the optical trapping potential. Five ms after the end of the BODT ramp, both MOT lights and gradient are switched off. Turning off the cooling light 20 μs before the repumper ones ensures the Cr component is in the $F_S = 9/2$ hyperfine ground state. After an additional hold time of 100 ms, we turn off the BODT and record, through an absorption image following a time-of-flight expansion, the number of Cr atoms collected in the trap.

The result of this characterization is summarized in Fig. 5, which shows the chromium number loaded into the optical trap, normalized to its maximum value, as a function of the power of the green light (blue circles). One can notice how, without the green beam, almost no atoms are collected in the

IR potential. By increasing the power of the 532-nm light instead, we observe a sharp enhancement of the atom number which, for our specific BODT beam parameters, reaches its maximum at $P_G = 0.47(1)$ W. A further increase of the green beam power beyond this optimum value progressively diminishes the Cr atom number. For $P_G \geqslant 1.25$ W, this approaches the value obtained by instantaneously flashing the IR trap right at the end of the CMOT stage, marked by the horizontal gray line in Fig. 5. This behavior can be understood by considering that, once the green light reaches this power level, atoms falling within the BODT volume are effectively transparent to the CMOT light and thus completely unaffected by it.

Owing to the strong inhomogeneity of the light shift experienced by the Cr CMOT atoms throughout the BODT region at the loading, it is hard to quantify the actual light shifts based on the method employed to characterize the IR beam at high temperature. Measurements performed in the ultracold regime, where the Cr sample is localized near the center of the green laser, yields a peak shift of $+38(5)$ MHz/W, characterized by a (positive) slope almost 2000 times larger than the IR (negative) one. Correspondingly, at the optimum value shown in Fig. 5, atoms residing at the center of the green beam experience an effective redshift of the cooling light of about -3.6Γ.

A quantitative analysis of the observed loading dynamics is quite involved and it goes beyond the scope of the present work. Anyway, we note a few qualitative, general facts. First, throughout the power range explored in Fig. 5, the green beam has a negligible impact on the total trap depth, which is solely set by the high-power IR beam. Second, depending on the specific laser source employed for realizing the green BODT beam, the optimum power may quantitatively move to higher or lower values, but the qualitative trend remains unaffected, as long as the wavelength of the green light remains close to, but shorter than, 532.9 nm. Third and most importantly, such a scheme leads to a substantial enhancement of the optical trapping efficiency, compared to the instantaneous flash of the IR beam, as it yields more than a fourfold improvement in the BODT atom number, and it does not cause any detectable excitation or heating of the atomic sample. Under optimum conditions, this strategy allows us to store up to 4×10^6 Cr atoms in the optical trap, at temperatures of about 250 μK, slightly lower than the typical CMOT one. Finally, we also remark that the absolute number of atoms that can be transferred into the BODT from the MOT with this strategy is found to scale linearly with the MOT atom number itself, as shown in Fig. 6: Up to the largest MOT clouds we can produce, we do not observe any saturation effect on the optically trapped samples, with a constant 5.5% MOT-to-BODT transfer efficiency. This observation demonstrates how our strategy indeed allows us to maintain light-assisted losses negligible up to the highest achievable densities, thereby making the ODT loading dynamics of chromium as simple as the one of lithium and other alkali metals.

Besides enabling the collection of a significant number of ^{53}Cr atoms, which may be appealing also for single-species setups dealing with cold (fermionic or bosonic) chromium, this direct loading method is especially advantageous in our mixture experiment. Indeed, the presence of the weak green laser field is essentially irrelevant for the loading of the lithium
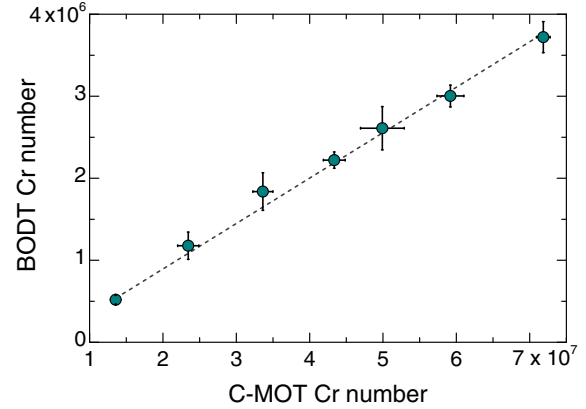

FIG. 6. Dependence of the number of chromium atoms collected in the BODT upon the CMOT atom number. The latter is adjusted by reducing the MOT loading time while not varying the MOT parameters. The IR beam is set to a power of 130 W and the green light is adjusted to the optimum value shown in Fig. 5. Data are recorded, after a hold time of 100 ms in the BODT, through absorption imaging that follows a time-of-flight expansion of 200 μs. Each point corresponds to the average value of at least four independent measurements of both CMOT and BODT numbers. Horizontal and vertical error bars represent the standard deviation of the mean. A linear fit to the data (see the dashed line) yields an overall MOT-to-BODT transfer efficiency of 5.5(2)%.

component: Up to 2×10^7 ^{6}Li atoms, with temperatures of about 280 μK, are stored in the BODT when the IR trap power is set to 130 W, with transfer efficiencies similar to those reported in Ref. [65] for the single-species case.

Since the two species feature similar temperatures, the simultaneous loading of the Li-Cr mixture in the BODT does not perturb too strongly the chromium performance, although the initial trap depth ratio, uniquely set by the IR beam, yields at 130 W $U_{\rm Li,IR} \sim 1.9$ mK and $U_{\rm Cr,IR} \sim 0.65$ mK, thus causing a rather large asymmetry in the temperature-to-trap-depth ratio between the two components. In fact, while $\eta_{\rm Li} = U_{\rm Li,IR}/k_B T_{\rm Li} \sim 7$, for chromium we obtain $\eta_{\rm Cr} = U_{\rm Cr,IR}/k_B T_{\rm Cr} \sim 3$. For this reason, the chromium BODT population, after a hold time of 100 ms, in the presence of the overlapping Li sample, is found to drop by almost a factor of 3. This effect is partly reduced by applying a 350-μs-long D_1 molasses phase on lithium within the BODT [65], about 3 ms after the end of the CMOT stage, once the magnetic-field quadrupole gradient has been zeroed. This allows us to reduce the lithium temperature, although not substantially, from 300 down to approximately 220 μK, a value slightly lower than the chromium one. At the end of the D_1 cooling, a 20-μs-long hyperfine pumping pulse is applied [65], which transfers all lithium atoms into the $F = 1/2$ ground-state manifold. Finally, within 20 ms the green power is linearly ramped up to its maximum value, corresponding to a net power of 6 W on the atoms, leading to about a 10% increase (6% decrease) of the chromium (lithium) trap depth.

The application of the BODT loading method for ^{53}Cr discussed above and its integration within our two-species experimental cycle allow us to store in our optical trap cold Li-Cr mixtures at about 250 μK, composed of 2×10^7 ^{6}Li atoms

populating the two lowest Zeeman states $m_F = \pm 1/2$ of the $F = 1/2$ manifold, coexisting with about 2×10^6 ^{53}Cr atoms, asymmetrically distributed among the four lowest-lying Zeeman state of the $F = 9/2$ hyperfine level. Specifically, without performing any Zeeman-selective optical pumping stage, we find that about 55% of the Cr sample is in the lowest Zeeman state $m_F = -9/2$. The remaining Cr atoms are distributed among the three higher-lying levels $m_F = -7/2, -5/2,$ and $-3/2$, with relative populations of 25%, 13%, and 7%, respectively. This represents our starting point for the successive stages of evaporative and sympathetic cooling, which we discuss in the following section. For convenience, in the following we denote the different Zeeman levels of both species by Li$|i\rangle$ and Cr$|i\rangle$, respectively, with $i = 1, 2, \ldots$ labeling the atomic state starting from the lowest-energy one.

IV. EVAPORATIVE AND SYMPATHETIC COOLING STAGES

Once the two species are loaded into the BODT, while the green BODT beam is ramped up to its maximum value, within 55 ms we also linearly increase the magnetic-field bias up to 880 G, i.e., about 50 G above the broad Feshbach resonance occurring between the two lowest Zeeman states of lithium Li$|1\rangle - Li|2\rangle$. At this field [7], intraspecies lithium collisions are unitarity limited at all temperatures relevant in this work, whereas interspecies Li-Cr collisions are at their background level, characterized by a scattering length $a_{bg} \sim 42a_0$ [48]. The magnetic-field curvature of our coils provides an additional in-plane harmonic confinement, characterized by a lithium (chromium) frequency of about 8.5 Hz (7.0 Hz), which adds to the BODT potential. The initial trap depth ratio between the two components $U_{Li}/U_{Cr} \sim 3$ and the comparably low initial value of $\eta_{Cr} \sim 3$ are not optimal for an efficient storage of chromium atoms in the presence of the lithium sample. For this reason, we find it experimentally convenient to start the evaporation immediately after the green beam has been raised.

The evaporative cooling ramps, overall lasting for about 5 s, are performed by decreasing the power of the BODT beams, hence the trap depth, through a series of exponential ramps, shown in Fig. 7(a) for the IR and green lights, respectively. Figures 7(b) and 7(c) show the corresponding evolution of the normalized atom number and temperature, for the Li$|1\rangle$ (red circles) and Cr$|1\rangle$ (blue circles) component, respectively, extracted from Gaussian fits to the density distributions, monitored via spin-selective absorption imaging following time-of-flight expansion. The Li$|2\rangle$ sample, not shown, throughout the evaporation stage is found at a temperature equal to the one of Li$|1\rangle$ and the corresponding atom number, relative to that of Li$|1\rangle$, is roughly constant at a value $N_{Li|2\rangle}/N_{Li|1\rangle} = 0.71(5)$. Additionally, Fig. 7(d) displays the ratio between the chromium and lithium temperatures throughout the evaporation stage.

During the first 400 ms, evaporative cooling of lithium is established by decreasing only the IR beam power, from 130 W down to 28 W. This first step, sufficiently slow to allow for intraspecies thermalization of lithium, is somewhat too fast for the chromium component, the temperature of which is found to be about 50% higher than the lithium one
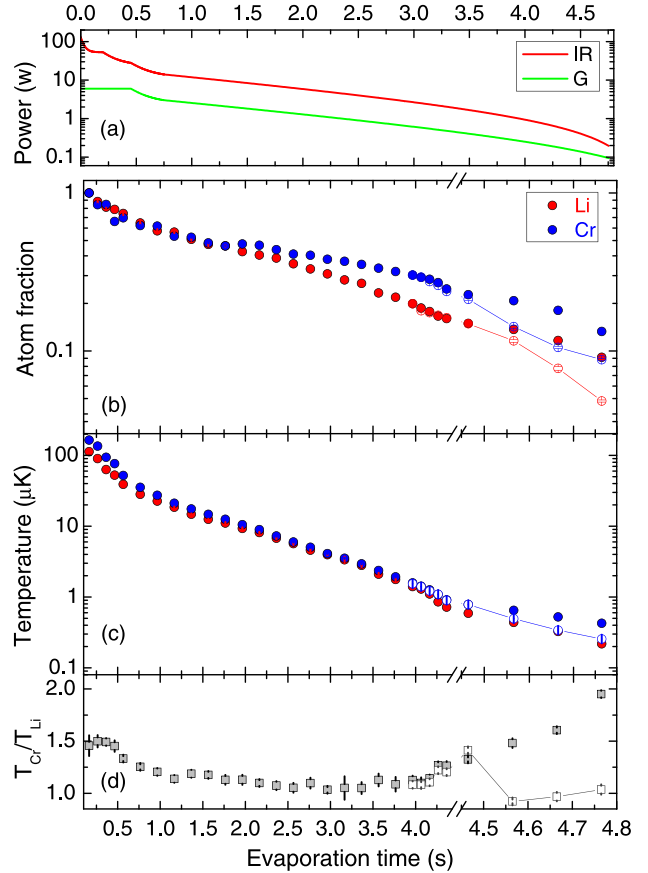

FIG. 7. (a) Evolution of the IR and green BODT powers during the evaporation ramp. The IR power is reduced through four consecutive exponential ramps, lasting 0.2, 0.25, 0.3, and 4 s, respectively, and characterized by $1/e$ decay times $\tau_1 = 30$ ms, $\tau_2 = 125$ ms, $\tau_3 = 150$ ms, and $\tau_4 = 1.6$ s. The green power is decreased through two consecutive ramps, simultaneous to the last two IR ones and featuring the same durations and decay times. (b) Evolution of the Li$|1\rangle$ (red circles) and Cr$|1\rangle$ (blue circles) atom number during the evaporation ramp. Both data sets are normalized to the atom numbers recorded after the first 165 ms of evaporation, where $N_{Li|1\rangle} = 5.1(1) \times 10^6$ and $N_{Cr|1\rangle} = 1.05(3) \times 10^6$. Open symbols refer to the number evolution when the Feshbach cooling stage is applied (see the text for details). (c) Same as in (b) but for Li and Cr temperatures. For both (b) and (c), numbers and temperatures are obtained from Gaussian fits to the atomic distributions, imaged after variable time-of-flight expansion. Note that, for the coldest samples, the temperature extracted from the Gaussian fit overestimates the real one, owing to Fermi degeneracy, up to about 40%. Each data point is the average of at least three independent measurements and error bars account for the standard deviation of the mean. Open symbols refer to the temperature evolution when the Feshbach cooling stage is applied. (d) Ratio between chromium and lithium temperatures, without (closed squares) and with (open squares) application of the Feshbach cooling stage.

[see Fig. 7(d)]. Despite the rather poor efficiency of sympathetic cooling observed within this initial stage, such a ramp allows us to rapidly diminish the U_{Li}/U_{Cr} ratio, from the initial value of 3 down to about 1. In order to maintain the chromium cloud well overlapped with the lithium one at all

times, we also minimize the differential gravitational sag of the two components by applying a magnetic-field gradient b along the vertical direction to counterbalance the gravitational force. Experimentally, we find an optimum value of about 1.6 G/cm, which corresponds to an almost perfect levitation of the chromium component and to an effective weak antigravity for lithium of about $-g/2$.

For evaporation times longer than 0.5 s, where $U_{Li}/U_{Cr} \sim 1$, the observed trajectories signal a good interspecies thermalization and a satisfactory sympathetic cooling. The observed decrease in atom number is indeed significantly smaller for the Cr than for the Li component [see Fig. 7(b)], while the chromium temperature closely follows the lithium one with less than 15% mismatch [see Figs. 7(c) and 7(d)], up to about 4 s. Here we obtain about 3×10^5 Cr$|1\rangle$ atoms at $T_{Cr} \sim 1.5 \, \mu$K, coexisting with about 1.1×10^6 Li$|1\rangle$ and 7.5×10^5 Li$|2\rangle$ atoms at $T_{Li} \sim 1.35 \, \mu$K, close to the onset of quantum degeneracy for both lithium components. By further decreasing the BODT trap depth following the trajectories shown in Fig. 7(a), we observe a progressive increase of T_{Cr}/T_{Li} [see Fig. 7(d)]. A convenient way to circumvent such a limited interspecies thermalization is offered by the presence of various s-wave Li-Cr Feshbach resonances, located at fields above 1400 G [48]. In particular, the Li$|1\rangle - Cr|1\rangle$ mixture possesses an approximately 0.5-G-wide Feshbach resonance at 1414 G and the Li$|2\rangle - Cr|1\rangle$ combination exhibits a resonance of similar character around 1461 G. Both features are immune to two-body losses [48] and, in spite of their relatively narrow character, allow us to magnetically control the Li-Cr scattering length a and thus to increase the Li-Cr elastic scattering cross section well above its background value.

In order to exploit such a possibility, about 1.5 s after the start of the evaporation stage, we linearly ramp the magnetic field from 880 G up to 2 G above the center of one of either resonances. There the Li-Cr scattering length is not significantly different from its background value $a \sim a_{bg}$ and also the intraspecies Li$|1\rangle - Li|2\rangle$ scattering length approaches its large and negative background value of about $-2500a_0$ [70]. About 4 s after the start of the evaporation, we then reduce the magnetic-field detuning to less than approximately 100 mG from the resonance center, correspondingly tuning the Li-Cr scattering length to $a \lesssim -200a_0$, yet not causing a significant enhancement of interspecies three-body losses. While a detailed characterization of such a Feshbach cooling mechanism near a narrow resonance is beyond the scope of the present study, the open symbols in Figs. 7(b)–7(d) highlight its impact on the final part of the evaporation ramps. One can see how, for fixed BODT power ramps, an increased Li-Cr scattering rate negligibly affects the Li temperature, whereas it causes a large decrease of the Cr one, allowing us to perfectly cancel the relative temperature mismatch [see the open squares in Fig. 7(d)]. The much quicker interspecies thermalization is accompanied by a more sizable atom loss of both species [see the blue (red) open circles in Fig. 7(b) for the Cr (Li) component]. However, this only moderately decreases the degree of degeneracy of lithium, while for chromium the atom loss is outweighed by the large temperature reduction, resulting in a substantial increase in the Cr phase-space density.

By following this protocol, overall lasting less than 5 s, we can produce degenerate Li-Cr Fermi mixtures, comprising up to 3.5×10^5 Li$|1\rangle$ and 2.5×10^5 Li$|2\rangle$ atoms at $T/T_{F,Li} \sim 0.25$, coexisting with about 10^5 Cr$|1\rangle$ atoms at $T/T_{F,Cr} \sim 0.5$. The corresponding degree of degeneracy $T/T_{F,i}$ is obtained by fitting time-of-flight images to finite-temperature Fermi-Dirac distributions. For both species, this is compatible with the value estimated on the basis of the measured atom number and trap frequencies ν_x, ν_y, and ν_z, within a 20% uncertainty equal to 16, 115, and 156 Hz and 13, 124, and 118 Hz for Li and Cr, respectively, and given the temperature $T = 130(20)$ nK, obtained by fitting the low-density wings of the atomic density distributions. Note that at the end of the evaporation the populations of the additional chromium minority components Cr$|i > 1\rangle$, initially loaded within the BODT, are negligible, owing to the combined effect of inelastic two-body losses occurring throughout the evaporation ramp and to the lack of thermalization with lithium, given the spin-selective character of the Feshbach cooling mechanism.

The evaporation trajectories summarized in Fig. 7(a) can be also adapted to produce single-species samples of either species. For lithium, this is straightforward: Without loading the chromium component, the same BODT power ramps discussed above yield crossover superfluids of more than 4.5×10^5 pairs when the bias field is tuned towards the pole of the broad intraspecies Feshbach resonance at 832 G. Such a number can be further increased up to about 6×10^5 when the same time evolution of the trap depth is realized by means of the sole IR light of the BODT, resulting in performances similar to, and even slightly better than, those reported in Ref. [65].

To realize polarized Fermi gases of ^{53}Cr, the protocols discussed above can be modified only partially, owing to the fact that quantum degeneracy of this species relies in our setup on sympathetic cooling with lithium. However, a slight increase of the green-to-IR power ratio during the evaporation allows us to obtain about 70% larger Cr samples at 220(20) nK, at the expense of a significant reduction of both Li components, which can be eventually completely removed at the end of the evaporation stage by further increasing the power of the green BODT arm. Sympathetic cooling of ^{53}Cr with ^{6}Li thus appears as a promising route to realize large Fermi gases of this yet poorly explored atomic species, so far produced only in combination with its most abundant bosonic isotope ^{52}Cr [60]. In fact, the possibility to exploit the different Li and Cr polarizabilities to the IR and green lights of our BODT, absent when isotopic Cr mixtures are considered, together with our substantially larger Cr MOT, allows for an almost 200-fold increase in the ^{53}Cr atom number that can be brought to $T/T_{F,Cr} \lesssim 1$, relative to previous studies [60].

V. INCREASING QUANTUM DEGENERACY IN A CROSSED BODT

As discussed in the preceding section, the degree of degeneracy, obtained at the end of the evaporation stage discussed therein, is quite different for the two mixture components, with lithium being highly degenerate while chromium features $T/T_{F,Cr} \sim 0.5$. Further decreasing the BODT trap depth does not lead to any substantial gain in phase-space density, a
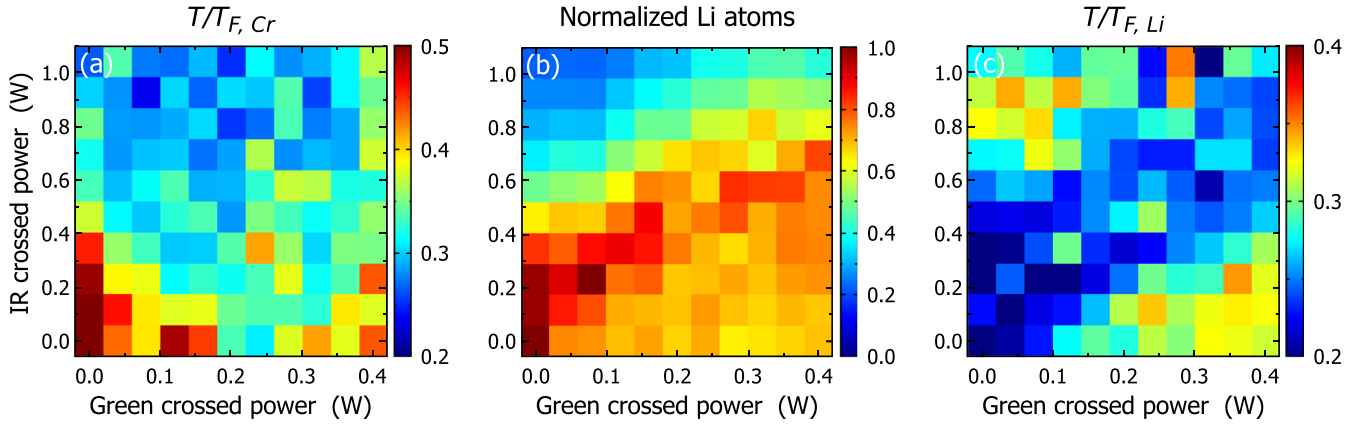
FIG. 8. (a) Normalized chromium temperature $T/T_{F,\mathrm{Cr}}$ monitored as a function of green and IR powers of the crossed BODT. The degree of degeneracy is obtained as the average value extracted from fitting at least four independent Cr images, acquired at a 4.6-ms time of flight. (b) Lithium atom number, normalized to its value measured in the sole main BODT at the end of the evaporation ramp, as a function of green and IR powers of the crossed BODT. (c) Same as in (a) but for the reduced lithium temperature $T/T_{F,\mathrm{Li}}$. For lithium, a 3-ms time-of-flight expansion was employed.

reduced temperature being counterbalanced by a drop in the atomic densities for both species.

To overcome this problem, once the evaporation stage has ended, we raise a second bichromatic trapping beam, which crosses the main BODT at an angle of about 15° from the vertical direction. Such a secondary beam is obtained by exploiting the same laser sources, recycling part of the IR and green powers of the main BODT, damped at the end of the evaporation procedure. Both IR and green crossed beams are almost circular and at the atom position they feature waists of about 60 and 70 μm, respectively. Being oriented almost vertically, such a second bichromatic beam does not modify the overall trap depth experienced by the two atomic components, and hence their temperature, whereas it allows us to control the confinement, and thus the density and Fermi energy, of each cloud almost independently.

In order to test this possibility, once the evaporation ramp is performed, we raise up the crossed BODT at various IR and green power levels through a 50-ms linear ramp. After about 50 ms, we then record time-of-flight images of both Li|1⟩ and Cr|1⟩ and obtain the corresponding atom number and degree of degeneracy by fitting the atomic clouds to a finite-temperature Fermi-Dirac distribution. The employed timings, although not exceeding the typical axial ones in the sole main BODT trap, do not cause any detectable excitation or trigger subsequent dynamics of the Li and Cr clouds. Exploitation of much longer ramp or hold times results instead in a poorer collection efficiency of the lithium component within the crossing region. The results of this characterization are summarized in the contour plots in Fig. 8: Figures 8(a) and 8(c) show the chromium and lithium normalized temperatures $T/T_{F,\mathrm{Cr}}$ and $T/T_{F,\mathrm{Li}}$, respectively, as a function of green and IR powers of the crossed beam. Figure 8(b) presents the corresponding trend for the Li|1⟩ atom number, normalized to 3.5×10^5, which is the value obtained without application of the crossed beam. The chromium component, characterized by an axial size in the main BODT roughly two times smaller than the lithium one, is efficiently transferred into the crossed

trap at all green and IR powers herein explored, resulting in a Cr number, not shown in Fig. 8, that varies less than 15% throughout the investigated parameter space.

One can notice the qualitatively different response of the two mixture components to the crossed BODT. On the one hand, for chromium, application of either crossed beam leads to a substantial increase in the degree of degeneracy: As shown in Fig. 8(a), several IR and green combinations yield a twofold decrease of $T/T_{F,\mathrm{Cr}}$, passing from about 0.5 down to 0.25, solely caused by the large Cr density increase within the crossed trap. On the other hand, for lithium, application of one single (IR or green) crossed beam causes a decrease of the atom number [see Fig. 8(b)] together with a reduction of the degree of degeneracy [see Fig. 8(c)]. The response to the IR trap can be explained by the initially larger cloud size and mean energy-to-trap depth ratio, compared to the Cr ones, which implies a limited collection efficiency and a progressively increased anharmonicity of the experienced potential, leading to a reduction of local density and degree of degeneracy. The response to the green crossed trap can instead be explained by the anticonfining (rather than confining) effect on the Li species: Even for low green powers, the atom-number reduction is accompanied by a drop of local density within the crossing region and hence of Fermi degeneracy.

However, when both IR and green lights are applied, over a quite wide range of parameters we observe an efficient storage of lithium atoms in the crossed BODT, at an almost constant $T/T_{F,\mathrm{Li}}$ [see Fig. 8(c)]. As expected, this occurs roughly around the diagonal of Figs. 8(b) and 8(c), where the anticonfinement of the green beam is (more than) counterbalanced by the IR light and where anharmonicities of the experienced potential, estimated through trap frequency measurements, appear to be negligible. These observations highlight how the crossed BODT significantly enhances the parameter space which can be explored with the Li-Cr mixture in our setup: By simply tuning the (absolute and relative) powers of the two crossed lights, one can pass from the regime
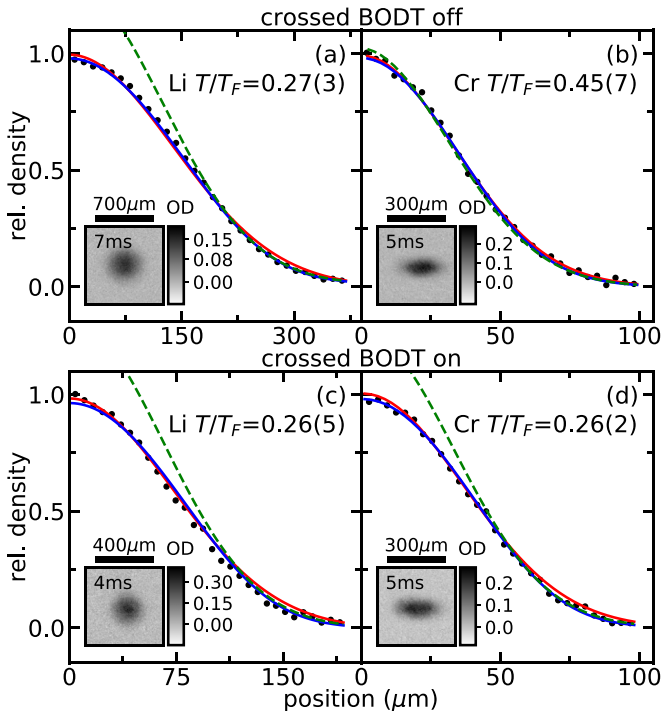
FIG. 9. Axially integrated density profiles (black circles) of (a) a lithium and (b) a chromium Fermi gas, simultaneously prepared in the main BODT trap only. Profiles are obtained from the average of about 20 independent absorption images, acquired after time-of-flight expansion and shown as insets. Experimental data are compared with best fits to a Fermi-Dirac (blue line) and a Gaussian (red line) distribution. A Gaussian fit to the low-density tails of the density distributions (green line) accurately captures the atom temperatures, whereas it overestimates the central density of highly degenerate samples. For each component, the reduced temperature T/T_F obtained from the former fit, together with the fit uncertainty, is specified in the panel. (c) and (d) Same as (a) and (b) but for a Li-Cr mixture released from a crossed BODT with IR and green powers set to (c) 0.81 and (d) 0.20 W. Application of such a crossed BODT does not alter the lithium degree of degeneracy, whereas it allows us to greatly reduce $T/T_{F,\mathrm{Cr}}$ and to obtain Li-Cr mixtures with both components at one-fourth of their Fermi temperature.

where lithium is highly degenerate and chromium is an almost thermal gas, to the opposite one.

Most importantly, over a sizable range of parameters we can simultaneously achieve a high degree of degeneracy for both ^{6}Li and ^{53}Cr components. As an example, in Fig. 9 we show axially integrated density profiles (black circles) of lithium and chromium Fermi gases, obtained from absorption images (see the insets), acquired after time-of-flight expansion from the sole main BODT trap [Figs. 9(a) and 9(b)] and from a crossed BODT [Figs. 9(c) and 9(d)]. Data are compared with best fits to a Gaussian and to a Fermi-Dirac distribution function, shown in red and blue, respectively. In both configurations, the lithium sample features a roughly constant and low $T/T_{F,\mathrm{Li}}$ value [see Figs. 9(a) and 9(c)] and a corresponding constant peak density of about 1×10^{12} cm^{-3}. For the chromium component, application of the crossed beam negligibly affects the gas temperature and the atom number, constantly about 1.0×10^5, while it greatly

modifies the peak density, which increases from slightly less than 2×10^{12} cm^{-3} in the sole main BODT to about 4×10^{12} cm^{-3} within the crossed trap. Correspondingly, the chromium degree of degeneracy is substantially improved, with the initial $T/T_{F,\mathrm{Cr}} = 0.45(7)$ being lowered to $0.26(2)$ [see Figs. 9(b) and 9(d)].

VI. CONCLUSION

We have reported on the experimental protocols that we devised to realize large and degenerate Fermi mixtures of lithium and chromium atoms. The present work, combined with our recent discovery and characterization of interspecies Li-Cr Feshbach resonances [48], makes ^{6}Li - ^{53}Cr mixtures an appealing playground with which to investigate a variety of yet unexplored phenomena, spanning from the few- and many-body physics of strongly interacting fermionic matter to the formation of paramagnetic polar molecules in the ultracold regime [56].

Owing to the peculiar chromium-lithium mass ratio, extremely close to the critical values above which non-Efimovian cluster states are predicted to emerge [9,13,15,18,37], our mixture may provide an exemplary benchmark for a wealth of theoretical predictions, lacking experimental observation in any physical system, so far. Moreover, the collisional stability predicted for such exotic few-body states [18,38,71] makes them appealing also from a many-body perspective. For instance, novel types of quasi-particles could emerge in the *light* impurity problem: Besides Fermi polarons and dressed dimers [72], lithium impurities embedded in a degenerate ^{53}Cr Fermi gas may indeed exhibit more complex quasiparticles [71,73,74], connected with the existence of higher-order few-body states in the vacuum. In this respect, the ability to widely tune both the degree of degeneracy and the relative densities of the Li and Cr components in our crossed BODT offers a compelling opportunity to investigate, within the same physical setup, both heavy and light impurity problems within fermionic media. Furthermore, our doubly degenerate mixture also appears optimally suited to investigate both *s*- and *p*-wave pairing and the possible emergence of superfluid states close to Li-Cr Feshbach resonances already identified [48].

The availability of large Li and Cr ultracold atomic gases, as well as the tunability of their densities enabled by our crossed bichromatic potential, provides a promising system to realize high phase-space density samples of bosonic Feshbach dimers [75,76], also in light of their increased collisional stability under strongly interacting conditions [77,78], when compared to those created from Fermi-Bose or Bose-Bose mixtures. The realization of a Bose-Einstein condensate of LiCr Feshbach dimers would not only pave the way to the exploration of resonant superfluidity with a mass-imbalanced Fermi mixture, but also would represent an optimal starting point to realize, through optical transfer schemes to deeply bound levels, degenerate Bose gases of paramagnetic molecules [56].

Finally, the experimental methods described in this work are appealing also to produce degenerate Fermi gases, or spin mixtures, of ^{53}Cr atoms: either via sympathetic cooling with lithium discussed herein or by adapting our strategies

to single-species setups. This fermionic species, yet almost unexplored, represents an interesting system on its own, as it combines a sizable magnetic dipole moment with a wide tunability of intraspecies interaction, enabled by broad and isolated Feshbach resonances, predicted for its two lowest Zeeman states [79,80]. As such, ^{53}Cr binary spin mixtures may offer a compelling opportunity to investigate the physics of the BCS-BEC crossover in the presence of weak dipolar interactions.

[1] R. Casalbuoni and G. Nardulli, Rev. Mod. Phys. **76**, 263 (2004).

[2] O. Andersen and L. Boeri, Ann. Phys. (Berlin) **523**, 8 (2011).

[3] H.-W. Hammer, A. Nogga, and A. Schwenk, Rev. Mod. Phys. **85**, 197 (2013).

[4] M. Yi, Y. Zhang, Z.-X. Shen, and D. Lu, npj Quantum Mater. **2**, 57 (2017).

[5] G. Wang, A. Chernikov, M. M. Glazov, T. F. Heinz, X. Marie, T. Amand, and B. Urbaszek, Rev. Mod. Phys. **90**, 021001 (2018).

[6] Y. Jiang, S. Chen, W. Zheng, B. Zheng, and A. Pan, Light Sci. Appl. **10**, 72 (2021).

[7] C. Chin, R. Grimm, P. Julienne, and E. Tiesinga, Rev. Mod. Phys. **82**, 1225 (2010).

[8] V. Efimov, Nucl. Phys. A **210**, 157 (1973).

[9] O. I. Kartavtsev and A. V. Malykh, J. Phys. B **40**, 1429 (2007).

[10] Y. Nishida and S. Tan, Phys. Rev. Lett. **101**, 170401 (2008).

[11] J. Levinsen, T. G. Tiecke, J. T. M. Walraven, and D. S. Petrov, Phys. Rev. Lett. **103**, 153202 (2009).

[12] Y. Castin, C. Mora, and L. Pricoupenko, Phys. Rev. Lett. **105**, 223201 (2010).

[13] S. Endo, P. Naidon, and M. Ueda, Few-Body Syst. **51**, 207 (2011).

[14] D. Blume, Rep. Prog. Phys. **75**, 046401 (2012).

[15] S. Endo, P. Naidon, and M. Ueda, Phys. Rev. A **86**, 062703 (2012).

[16] V. Ngampruetikorn, M. M. Parish, and J. Levinsen, Europhys. Lett. **102**, 13001 (2013).

[17] J. Levinsen and M. M. Parish, Phys. Rev. Lett. **110**, 055304 (2013).

[18] B. Bazak and D. S. Petrov, Phys. Rev. Lett. **118**, 083002 (2017).

[19] B. Bazak, Phys. Rev. A **96**, 022708 (2017).

[20] R. Liu, C. Peng, and X. Cui, Phys. Rev. Lett. **129**, 073401 (2022).

[21] W. V. Liu and F. Wilczek, Phys. Rev. Lett. **90**, 047002 (2003).

[22] M. M. Forbes, E. Gubankova, W. V. Liu, and F. Wilczek, Phys. Rev. Lett. **94**, 017001 (2005).

[23] M. Iskin and C. A. R. Sá de Melo, Phys. Rev. Lett. **97**, 100404 (2006).

[24] M. M. Parish, F. M. Marchetti, A. Lamacraft, and B. D. Simons, Nat. Phys. **3**, 124 (2007).

[25] M. A. Baranov, C. Lobo, and G. V. Shlyapnikov, Phys. Rev. A **78**, 033620 (2008).

[26] K. B. Gubbels, J. E. Baarsma, and H. T. C. Stoof, Phys. Rev. Lett. **103**, 195301 (2009).

[27] A. Gezerlis, S. Gandolfi, K. E. Schmidt, and J. Carlson, Phys. Rev. Lett. **103**, 060403 (2009).

[28] J. E. Baarsma, K. B. Gubbels, and H. T. C. Stoof, Phys. Rev. A **82**, 013624 (2010).

[29] K. Gubbels and H. Stoof, Phys. Rep. **525**, 255 (2013).

[30] J. Wang, Y. Che, L. Zhang, and Q. Chen, Sci. Rep. **7**, 39783 (2017).

[31] M. Pini, P. Pieri, R. Grimm, and G. C. Strinati, Phys. Rev. A **103**, 023314 (2021).

[32] C. W. von Keyserlingk and G. J. Conduit, Phys. Rev. A **83**, 053625 (2011).

[33] A. Sotnikov, D. Cocks, and W. Hofstetter, Phys. Rev. Lett. **109**, 065301 (2012).

[34] A. Sotnikov, M. Snoek, and W. Hofstetter, Phys. Rev. A **87**, 053602 (2013).

[35] P. Massignan, Z. Yu, and G. M. Bruun, Phys. Rev. Lett. **110**, 230401 (2013).

[36] X. Cui and T.-L. Ho, Phys. Rev. Lett. **110**, 165302 (2013).

[37] D. Blume, Phys. Rev. Lett. **109**, 230404 (2012).

[38] J. Levinsen and D. S. Petrov, Eur. Phys. J. D **65**, 67 (2011).

[39] P. Naidon and S. Endo, Rep. Prog. Phys. **80**, 056001 (2017).

[40] E. Wille, F. M. Spiegelhalder, G. Kerner, D. Naik, A. Trenkwalder, G. Hendl, F. Schreck, R. Grimm, T. G. Tiecke, J. T. M. Walraven, S. J. J. M. F. Kokkelmans, E. Tiesinga, and P. S. Julienne, Phys. Rev. Lett. **100**, 053201 (2008).

[41] A.-C. Voigt, M. Taglieber, L. Costa, T. Aoki, W. Wieser, T. W. Hänsch, and K. Dieckmann, Phys. Rev. Lett. **102**, 020405 (2009).

[42] L. Costa, J. Brachmann, A.-C. Voigt, C. Hahn, M. Taglieber, T. W. Hänsch, and K. Dieckmann, Phys. Rev. Lett. **105**, 123201 (2010).

[43] C. Ravensbergen, V. Corre, E. Soave, M. Kreyer, E. Kirilov, and R. Grimm, Phys. Rev. A **98**, 063624 (2018).

[44] C. Ravensbergen, E. Soave, V. Corre, M. Kreyer, B. Huang, E. Kirilov, and R. Grimm, Phys. Rev. Lett. **124**, 203402 (2020).

[45] H. Hara, Y. Takasu, Y. Yamaoka, J. M. Doyle, and Y. Takahashi, Phys. Rev. Lett. **106**, 205304 (2011).

[46] A. Green, H. Li, J. H. See Toh, X. Tang, K. C. McCormick, M. Li, E. Tiesinga, S. Kotochigova, and S. Gupta, Phys. Rev. X **10**, 031037 (2020).

[47] M. Jag, M. Zaccanti, M. Cetina, R. S. Lous, F. Schreck, R. Grimm, D. S. Petrov, and J. Levinsen, Phys. Rev. Lett. **112**, 075302 (2014).

[48] A. Ciamei, S. Finelli, A. Trenkwalder, M. Inguscio, A. Simoni, and M. Zaccanti, Phys. Rev. Lett. **129**, 093402 (2022).

[49] D. S. Petrov, Phys. Rev. A **67**, 010703(R) (2003).

[50] E. Stoner, Philos. Mag. **15**, 1018 (1933).

[51] G.-B. Jo, Y.-R. Lee, J.-H. Choi, C. A. Christensen, T. H. Kim, J. H. Thywissen, D. E. Pritchard, and W. Ketterle, Science **325**, 1521 (2009).

[52] F. Scazza, G. Valtolina, P. Massignan, A. Recati, A. Amico, A. Burchianti, C. Fort, M. Inguscio, M. Zaccanti, and G. Roati, Phys. Rev. Lett. **118**, 083602 (2017).

[53] G. Valtolina, F. Scazza, A. Amico, A. Burchianti, A. Recati, T. Enss, M. Inguscio, M. Zaccanti, and G. Roati, Nat. Phys. **13**, 704 (2017).

[54] A. Amico, F. Scazza, G. Valtolina, P. E. S. Tavares, W. Ketterle, M. Inguscio, G. Roati, and M. Zaccanti, Phys. Rev. Lett. **121**, 253602 (2018).

[55] F. Scazza, G. Valtolina, A. Amico, P. E. S. Tavares, M. Inguscio, W. Ketterle, G. Roati, and M. Zaccanti, Phys. Rev. A **101**, 013603 (2020).

[56] K. Zaremba-Kopczyk, M. Gronowski, and M. Tomza, Ultracold mixtures of Cr and Li atoms Theoretical prospects for controlled atomic collisions, LiCr molecule formation, and molecular precision measurements (to be published).

[57] F. M. Spiegelhalder, A. Trenkwalder, D. Naik, G. Kerner, E. Wille, G. Hendl, F. Schreck, and R. Grimm, Phys. Rev. A **81**, 043637 (2010).

[58] E. Neri, A. Ciamei, C. Simonelli, I. Goti, M. Inguscio, A. Trenkwalder, and M. Zaccanti, Phys. Rev. A **101**, 063602 (2020).

[59] R. Chicireanu, A. Pouderous, R. Barbé, B. Laburthe-Tolra, E. Maréchal, L. Vernac, J.-C. Keller, and O. Gorceix, Phys. Rev. A **73**, 053406 (2006).

[60] B. Naylor, A. Reigue, E. Maréchal, O. Gorceix, B. Laburthe-Tolra, and L. Vernac, Phys. Rev. A **91**, 011603(R) (2015).

[61] R. Chicireanu, Q. Beaufils, A. Pouderous, B. Laburthe-Tolra, É. Maréchal, L. Vernac, J.-C. Keller, and O. Gorceix, Eur. Phys. J. D **45**, 189 (2007).

[62] Q. Beaufils, R. Chicireanu, T. Zanon, B. Laburthe-Tolra, E. Maréchal, L. Vernac, J.-C. Keller, and O. Gorceix, Phys. Rev. A **77**, 061601(R) (2008).

[63] D. Naik, A. Trenkwalder, C. Kohstall, F. M. Spiegelhalder, M. Zaccanti, G. Hendl, F. Schreck, R. Grimm, T. M. Hanna, and P. S. Julienne, Eur. Phys. J. D **65**, 55 (2011).

[64] C. Simonelli, E. Neri, A. Ciamei, I. Goti, M. Inguscio, A. Trenkwalder, and M. Zaccanti, Opt. Express **27**, 27215 (2019).

[65] A. Burchianti, G. Valtolina, J. A. Seman, E. Pace, M. De Pas, M. Inguscio, M. Zaccanti, and G. Roati, Phys. Rev. A **90**, 043408 (2014).

[66] H. J. Metcalf and P. van der Straten, *Laser Cooling and Trapping* (Springer, New York, 1999).

[67] F. P. D. Santos, F. Perales, J. Léonard, A. Sinatra, J. Wang, F. S. Pavone, E. Rasel, C. S. Unnikrishnan, and M. Leduc, Eur. Phys. J. Appl. Phys. **14**, 69 (2001).

[68] R. Chang, A. L. Hoendervanger, Q. Bouton, Y. Fang, T. Klafka, K. Audo, A. Aspect, C. I. Westbrook, and D. Clément, Phys. Rev. A **90**, 063407 (2014).

[69] G. Bismut, B. Pasquiou, D. Ciampini, B. Laburthe-Tolra, E. Maréchal, L. Vernac, and O. Gorceix, Appl. Phys. B **102**, 1 (2011).

[70] G. Zürn, T. Lompe, A. N. Wenz, S. Jochim, P. S. Julienne, and J. M. Hutson, Phys. Rev. Lett. **110**, 135301 (2013).

[71] S. Endo, A. M. García-García, and P. Naidon, Phys. Rev. A **93**, 053611 (2016).

[72] P. Massignan, M. Zaccanti, and G. M. Bruun, Rep. Prog. Phys. **77**, 034401 (2014).

[73] C. J. M. Mathy, M. M. Parish, and D. A. Huse, Phys. Rev. Lett. **106**, 166404 (2011).

[74] R. Liu, C. Peng, and X. Cui, Cell Rep. Phys. Sci. **3**, 100993 (2022).

[75] M. Duda, X.-Y. Chen, A. Schindewolf, R. Bause, J. von Milczewski, R. Schmidt, I. Bloch, and X.-Y. Luo, arXiv:2111.04301.

[76] A. Z. Lam, N. Bigagli, C. Warner, W. Yuan, S. Zhang, E. Tiemann, I. Stevenson, and S. Will, Phys. Rev. Res. **4**, L022019 (2022).

[77] D. S. Petrov, C. Salomon, and G. V. Shlyapnikov, Phys. Rev. Lett. **93**, 090404 (2004).

[78] M. Jag, M. Cetina, R. S. Lous, R. Grimm, J. Levinsen, and D. S. Petrov, Phys. Rev. A **94**, 062706 (2016).

[79] Z. Pavlovic, Dipolar collisions in cooling and trapping of paramagnetic atoms, Ph.D. thesis, University of Connecticut, 2011.

[80] A. Simoni (private communication 2022).